Journal of Power Sources 195 (2010) 4059–4064

Contents lists available at ScienceDirect

Journal of Power Sources

journal homepage: www.elsevier.com/locate/jpowsour

Ionic conductivity of apatite-type solid electrolyte material, $La_{10-X}Ba_XSi_6O_{27-X/2}$ ($X = 0–1$), and its fuel cell performance

Y. Nojiri[b,*], S. Tanase[a], M. Iwasa[a], H. Yoshioka[c], Y. Matsumura[a], T. Sakai[a]

[a] National Institute of Advanced Industrial Science and Technology (AIST), Kansai Center, 1-8-31 Midorigaoka Ikeda, Osaka 563-8577, Japan
[b] International Research Center for Hydrogen Energy, Kyushu University, 744 Motooka, Nishi-ku, Fukuoka 819-0395, Japan
[c] Hyogo Prefectural Institute of Technology, 3-1-12 Yukihira-cho, Suma-ku, Kobe 654-0037, Japan

ARTICLE INFO

Article history:
Received 16 October 2009
Received in revised form 18 January 2010
Accepted 22 January 2010
Available online 6 February 2010

Keywords:
Solid oxide fuel cell
Electrolyte
Lantanum silicate
Apatite-type oxide
$La_{10}Si_6O_{27}$

ABSTRACT

We prepared Ba substituted lanthanum silicate ($La_{10-X}Ba_XSi_6O_{27-X/2}$) and examined the effect of Ba substitution on the crystal structure and conductivity. The X-ray diffraction (XRD) results for a series of compositions showed that Ba ion can occupy the La site of an apatite structure with the composition $La_{10-X}Ba_XSi_6O_{27-X/2}$ ($X = 0–1$). Rietveld analysis of the synchrotron XRD profiles revealed Ba occupation in the La 4f site rather than the La 6 h site and a decrease in the occupation factors of the oxide ions of the SiO_4 tetrahedra.

The conductivity of $La_{10-X}Ba_XSi_6O_{27-X/2}$ exhibited a maximum at $X = 0.6$ and the value was the same as that of YSZ (8 mol% Y_2O_3 doped ZrO_2) at 750 °C. On the other hand, the activation energy of about 50 kJ mol^{-1} for $La_{9.4}Ba_{0.6}Si_6O_{26.7}$ was smaller than that of YSZ. Thus the conductivity of $La_{9.4}Ba_{0.6}Si_6O_{26.7}$ was a higher than those of YSZ below 750 °C. The conductivity parallel to the c-axis which is attributed to the 2a site oxide ions migration is known to be dominant in $La_{10}Si_6O_{27}$. However, Ba substitution seems to produce oxygen vacancies and create another pathway for oxide ions perpendicular to the *c*-axis. The increase in the pathways leads to an increase in the conductivity. We also reported the solid oxide fuel cell (SOFC) performance of $La_{10-X}Ba_XSi_6O_{27-X/2}$ with a maximum power density of 65 mW cm^{-2} using $La_{0.9}Sr_{0.1}CoO_{3-\delta}$ as a cathode and NiO-SDC (Sm doped CeO_2) as an anode.

1. Introduction

The fuel cell is expected to be used as a clean power source in many fields. Polymer electrolyte fuel cells (PEFCs), molten carbonate fuel cells (MCFCs), and many other types of fuel cells are now being proposed. These fuel cells, especially the solid oxide fuel cells (SOFCs), are able to obtain higher power generation efficiency and can use a variety of fuels. However, the operating temperature of an SOFC is around 1000 °C, which is too high for the material stability under long-term operation and for quick starting and stopping of the cell. Therefore, it is necessary to improve the conductivity of the electrolyte material at low temperatures to decrease the operating temperature of the cell. YSZ (Y_2O_3 doped ZrO_2), GDC (Gd_2O_3 doped CeO_2), and LSGM ($La_{0.8}Sr_{0.2}Ga_{0.8}Mg_{0.2}O_{2.8}$) are electrolyte candidates for fuel cells [1]. Among these materials, YSZ and GDC have a fluorite-type structure and LSGM has a perovskite-type structure. In addition to these oxides, $La_{10}Si_6O_{27}$, which has an apatite structure, has recently attracted much attention as a new electrolyte for SOFCs [2–11]. The conduction mechanism of this oxide is the interstitial diffusion of oxide ions. This type of conduction is totally different from that of conventional oxides such as fluorite oxides, with the mechanism known as the vacancy diffusion mechanism. From a crystallographic view point, the apatite structure can be described as $A_{10}(BO_4)_6X_2$ (A: lanthanides, alkaline earth elements; B: Al, Si, P, Ge, Ga, etc.; X: O, OH, CO_3, F). Based on the charge neutrality, the crystal structure of $La_{10}Si_6O_{27}$ is based on $La_{9.33}Si_6O_{26}$, which does not have any interstitial oxygen [14,24]. As the number of La ions in the La sites increases, excess oxygen ions are introduced into the interstitial oxide-ion sites of the crystal, which results in an increase in the conductivity. The conductivity reported for pure (undoped) lanthanum silicate is the highest for $La_{10}Si_6O_{27}$ [2–7,16]. This type of oxide was known as a pure oxide-ion conductor under 800 °C, without phase transition [3,7,25–27]. In an experiment with a single crystal sample the conductivity was 16 times larger in the *c*-axis direction than in the other directions [14]. This result also shows the existence of a-axis conduction in $La_{9.33}Si_6O_{26}$.

La ions in this material can be substituted by other rare earth elements [2–7] or alkaline earth elements [12–15,24]. These investigations showed that substitution by the rare earth elements did not improve the conductivity, while the Sr substitution on the La site improved conductivity [7]. The Si site of $La_{10}Si_6O_{27}$ is sub-

* Corresponding author. Tel.: +81 92 802 3094; fax: +81 92 802 3094.
E-mail address: y-nojiri@mech.kyushu-u.ac.jp (Y. Nojiri).

0378-7753/$ – see front matter © 2010 Elsevier B.V. All rights reserved.
doi:10.1016/j.jpowsour.2010.01.050

stitutable with transition metals and Al, Ga, and Ge [11–15,22]. Furthermore, it has been reported that a small amount of Mg can be substituted in the Si site of $La_{9.67}Si_6O_{27}$, which indicates that alkaline earth elements do not always occupy the La sites [16,17,23]. Recently, La site substitution was carried out for $La_9MSi_6O_{26.5}$ (M = Ca, Sr, and Ba). In this case, the authors determined that the synthesizing temperature was 1650 °C from the sintered density and shrinkage of the samples [18–20]. Lattice parameters of these samples were calculated from the XRD patterns, but the lattice parameter of the a-axis did not follow the Vegard's law. In addition, there was no optimization of the substitution amount [17–20]. There are no reports about the relationship between the substitution site and conductivity.

In this study, we paid attention to the Ba ion which has the large ionic radii among the alkaline earth elements. We examined the substitution characteristics of the La sites with Ba ions and calculated the lattice parameter using the internal standard method with the XRD results. A Rietveld analysis was carried out using the X-ray powder diffraction patterns of the synchrotron radiation to refine the lattice parameter and Ba^{2+} occupation sites. We here report the relation between the crystallographic parameters on the Ba substitution and the conductivities to discuss the conduction mechanism of the oxide ion. We will also report the fuel cell performances of the lanthanum silicates.

2. Experimental

The samples were obtained by the solid-state reaction method. The starting materials were La_2O_3 (Kishida Chemical Co., 99.99%), SiO_2 (Kishida Chemical Co., 99%), and $BaCO_3$ (CERAC Inc., 99.999%). These materials were weighed out as $La_{10-X}Ba_XSi_6O_{27-X/2}$ (X = 0–1.0) and mixed using an automatic alumina mortar. The mixture were pressed into a pellets. The pellets were placed on a Pt plate to avoid any reaction with an alumina boat and then heated at 1650 °C for 20 h. Next, the samples were crushed into powder, and reformed into a pellets, and calcined at 1650 °C for another 20 h again. Finally, the sample was ground in a mortar and again reshaped into a pellets. Then, a cold isotropic press (CIP) process was carried out on the processed pellets at 200 MPa and the pellets were sintered at 1680 °C for 10 h.

To confirm the chemical composition, an inductively coupled plasma (ICP) analysis of each sample was carried out using an IRIS Advantage ICP-AES system (Nippon Jarrell-Ash Co., Ltd.). The ICP data showed that the composition was almost the same as the initial composition.

Phase characterization was carried out by XRD (Mac Science $M06X^{CE}$) using Cu Kα radiation. The lattice parameter of each sample was determined by the internal standard method. Si powder (Kishida Chemical Co., 99.999%) was used as an internal standard.

Synchrotron XRD patterns were obtained to distinguish the Ba ion occupation sites in the La sites at the synchrotron radiation facility SPring-8, Japan, using BL19B2, which is a medium-length hard X-ray bending magnet beamline designed for engineering science research. A large Debye–Scherrer camera was used to perform a precise structural analysis of the powder diffraction patterns. The camera has a radius of 286.5 mm and an imaging plate (IP) on the 2θ arm that acted as a detector. The diffraction patterns were recorded in the 2θ range of 1–75°, and a selected pixel size of the IP was 50 μm. The sample was loaded into a glass capillary (D = 0.3 mm) and irradiated by the synchrotron X-ray while rotating the samples to improve the homogeneity. The observed X-ray diffraction pattern was fitted by using the Rietveld program (REITAN-2000) to refine the structural parameters [31]. The X-rays had a wavelength of 0.75 Å, which was detected using CeO_2 as a standard. The X-ray exposure time was 300 s for each sample.

To measure the electrical conductivity, the sintered samples were cut into rectangles and the four Pt wire were attached to each sample with uniform separations. The electrical conductivity was measured by the four probe method using an impedance analyzer (Solartron 1260) and an electrochemical interface (Solartron 1286) at different temperatures from 500 to 1000 °C in an ambient atmosphere.

The fuel cell testing was performed using 1-mm thick disk-shaped samples. $La_{0.9}Sr_{0.1}CoO_{3-\delta}$ was used for the cathode and NiO-SDC (NiO:Sm doped CeO_2 = 70:30 by wt%) was used for the anode. These powdered electrode materials ware separately dispersed in terpineol and painted on each side of the electrolyte, which was then calcined at 1300 °C for 3 h. The measurement temperature was 800 °C. Air and moisturized H_2 gas were introduced to the cathode and anode, respectively. The water vapor pressure was controlled using a saturation temperature of 30 °C. A flow rate of 50 cm^3 min^{-1} was used for both gases.

3. Results and discussion

3.1. Crystal structure analysis

The XRD patterns of the samples are shown in Fig. 1. All of the samples were identified as a single apatite phase which is identical with $La_{10}Si_6O_{27}$. No impurity peaks were observed in the XRD patterns. These results indicate that the Ba ions in all of the sam-

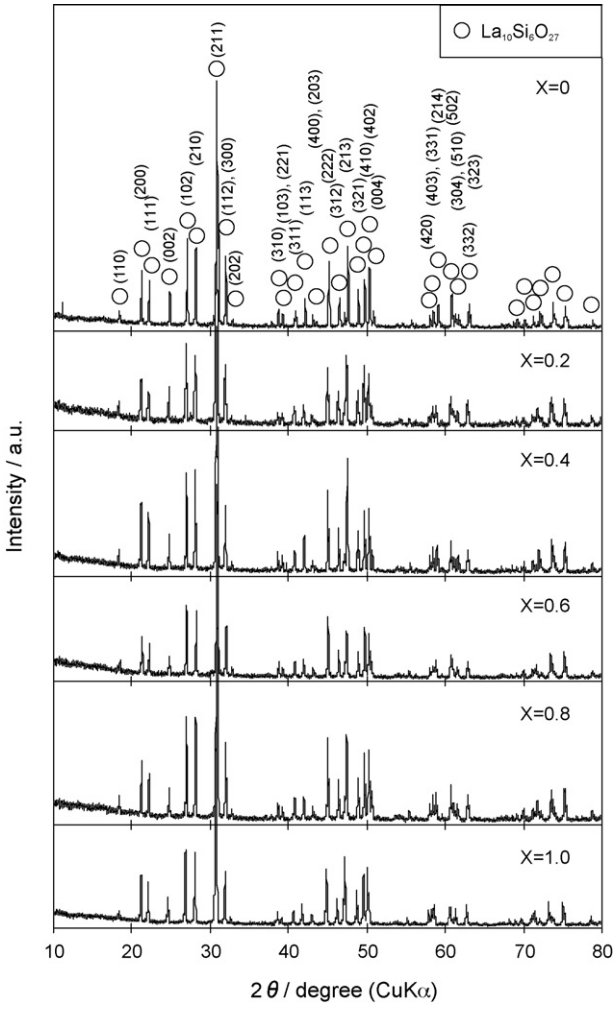

Fig. 1. The observed XRD patterns of the $La_{10-X}Ba_XSi_6O_{27-X/2}$ (X = 0–1) samples.

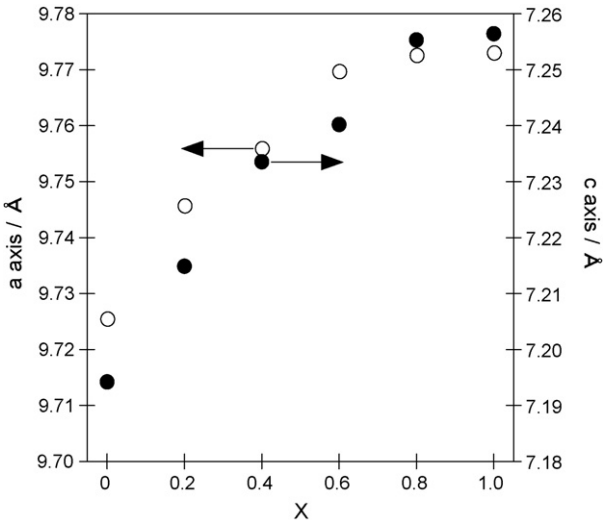

Fig. 2. The lattice parameter of $La_{10-X}Ba_XSi_6O_{27-0.5X}$.

ples were fully substituted. Fig. 2 shows the lattice parameters of the Ba-substituted samples, which were obtained using the internal standard method. Both the *a*-axis and *c*-axis lattice parameters of the samples increases with the amount of substituted Ba. These results can be explained by the isotropic expansion of the samples from the ionic radius difference between Ba^{2+} (1.36 Å) and La^{3+} (1.06 Å). However, the lattice parameters of $X > 0.6$ do not change linearly with *X*. With these results of $X > 0.6$, the formation of a glass phase was suspected. However, from the phase diagram of $BaO–SiO_2$ system, the $BaO–SiO_2$ glass will melt at the sample composition and synthesize temperature [28,29]. If, the glass phase was formed, the sample can be sintered at below 1400 °C by liquid phase sintering. Since the Ba substituted lanthanum silicate is difficult to be sintered below 1600 °C, there is a little possibility of the glass phase formation. One possible explanation for this result is a change in the substituted site of Ba ions from the La 4f to the 6h with $X > 0.6$. The coordination numbers of the La 4f and the La 6h sites are 9 and 7, respectively. When the Ba ion substitute at the La 6h site, a difference in the coordination number from the La 4f site may cause the change in the lattice parameter [20].

Fig. 3 shows fitting of the diffraction patterns of the $La_{10}Si_6O_{27}$ and $La_{9.4}Ba_{0.6}Si_6O_{26.7}$ which were measured by synchrotron X-ray and refined by the Rietveld analysis. The refined parameters of $La_{10}Si_6O_{27}$ and $La_{9.4}Ba_{0.6}Si_6O_{26.7}$ are shown in Table 1. The refined crystal structure of $La_{10}Si_6O_{27}$ is shown in Fig. 4. The sample symmetry used for the refinement was $P6_3/m$ (No. 176). As shown in Fig. 4, the cation structure of $La_{10}Si_6O_{27}$ consists of alternately layered triangles formed by the La 6h and Si 6h. The La 4f site is located between the La and Si triangles. Oxide ions occupy five different sites, three of which are located close to the Si site (O1 6h, O2 6h, O3 12i) with one oxide-ion site locating at the corner of the unit cell (O4 2a). The interstitial oxide ion is located in the middle of O4 2a and O3 12i (O5 12i). The La 6h site and La 4f site are two substitutable sites for Ba^{2+}. The fitting result (R_{wp}) for the model with Ba ions substituted in the La 4f site is 8.46%, as shown in Table 1, which is lower than the model with the La 6h site substitution (8.68%). The result for the Ba substitution site is in agreement with a recent report on Ba-substituted $La_{10}Si_6O_{27}$ [20].

All occupation factors of the oxide ions decreased slightly in the Ba-substituted sample, except for O5 12i. For the SiO_4 tetrahedra in $La_{9.4}Ba_{0.6}Si_6O_{26.7}$, the occupation factors of the oxide ions are 0.9850, as shown in Table 1. This result indicates that oxide ions did not fully occupy the SiO_4 tetrahedra in the Ba substituted samples. The oxide ion of the SiO_4 tetrahedra also constitutes an oxygen

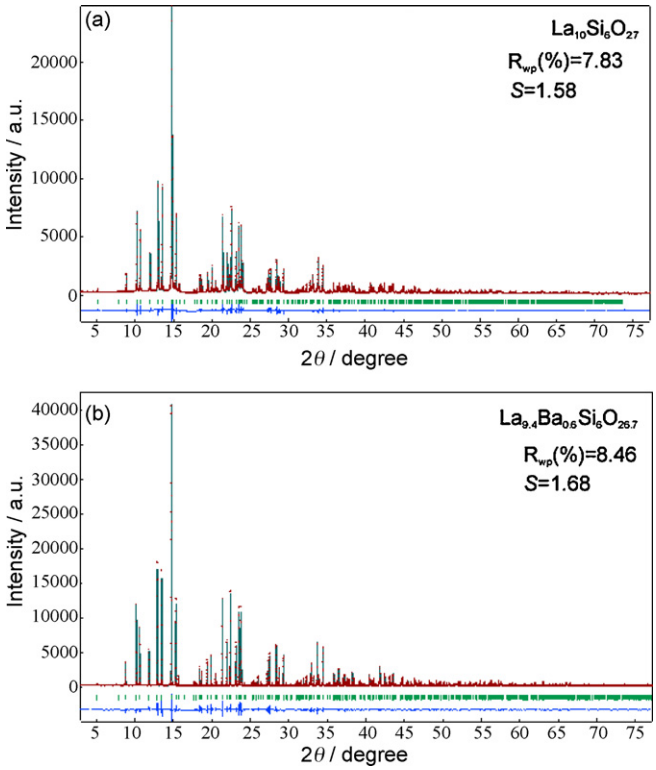

Fig. 3. The observed and calculated patterns from Rietveld refinements of $La_{10}Si_6O_{27}$ and $La_{9.4}Ba_{0.6}Si_6O_{26.7}$. The measurements of the observed patterns were carried out by using synchrotron radiation at SPring 8 (BL19B2).

site of La_2O_3, which suggests that a SiO_4 tetrahedra does not exist independently in the crystal. From this reason, interaction between a La and Si ions through an oxygen ion produces a small oxygen defect at the SiO_4 tetrahedra by the Ba substitution of the La 4f site. The XRD pattern of $X = 0.8$ was refined by the Rietveld analysis

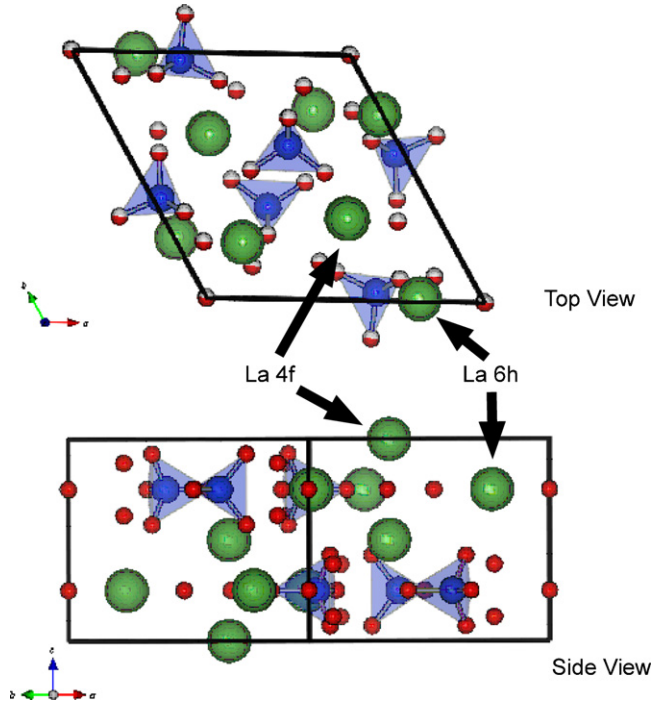

Fig. 4. The crystal structure of $La_{10}Si_6O_{27}$. This structure was determined from the results of the synchrotron radiation.

Table 1
Refined structural parameters for $La_{10}Si_6O_{27}$ and $La_{9.4}Ba_{0.6}Si_6O_{26.7}$.

	$La_{10}Si_6O_{27}$	$La_{9.4}Ba_{0.6}Si_6O_{26.7}$
a (Å)	9.7255	9.7698
c (Å)	7.1943	7.2402
V (Å^3)	589.31	598.48
R_{wp} (%)	7.83	8.46
R_I (%)	3.17	2.28
S	1.58	1.68
La1, 6h (*x y* 1/4)		
x	0.22862(2)	0.22749(3)
y	0.01121(2)	0.01183(5)
B (Å)	0.694(1)	0.756(5)
La2, 4f (1/3 2/3 *z*)		
g	0.8500	
z	0.00061(1)	0.00092(1)
B (Å)	1.620(7)	1.235(5)
Ba 4f (1/3 2/3 *z*)		
g	0	0.1500
z	= z (La 4f)	= z (La 4f)
B (Å)	=*B* (La 4f)	0.185(7)
Si 6h (*x y* 1/4)		
x	0.40296(4)	0.40098(1)
y	0.37232(4)	0.37233(1)
B (Å)	0.304(2)	0.073(1)
O1 6h (*x y* 1/4)		
g	0.9937(6)	0.9850(1)
x	0.32527(4)	0.32252(4)
y	0.48099(3)	0.47958(4)
B (Å)	0.632(1)	1.669(5)
O2 6h (*x y* 1/4)		
g	0.9937(6)	0.9850(1)
x	0.58820(3)	0.59166(5)
y	0.47495(3)	0.47275(4)
B (Å)	0.636(1)	1.149(4)
O3 12i (*x y z*)		
g	0.9937(6)	0.9850(1)
x	0.34769(4)	0.34368(2)
y	0.26008(4)	0.25866(2)
z	0.07536(3)	0.07394(2)
B (Å)	0.638(1)	2.419(1)
O4 2a (0 0 1/4)		
g	0.97(1)	0.930(7)
B (Å)	0.668(2)	1.490(2)
O5 12i (0.1 0.23 0.62)		
g	0.100(1)	0.100(6)
B (Å)	0.600(5)	1.494(3)

based on the different structural models of the Ba substitution sites. The fitting index, R_{wp}, for the model in which Ba ions substitutes both La 6h and 4f sites, is 14.6%, which is smaller than the model in which all Ba ions substitute the La 4f site only (R_{wp} = 17.1%). The result supports the above idea.

3.2. Conductivity

Fig. 5 shows the temperature dependence of the bulk conductivities of the Ba-substituted samples in comparison with 8YSZ (8 mol% Y_2O_3 substituted ZrO_2). The bulk conductivity of $La_{10}Si_6O_{27}$ (X = 0) is higher than YSZ below 670 °C and has an inflection point at 743 °C, which suggests a change in the conduction mechanism. Such an inflection point is sometimes attributed to a phase transition [21] or a change in an electronic contribution to the conductivity. Since $La_{10}Si_6O_{27}$ is reported to be a pure ionic conductor without a phase transition in this temperature range, the inflection point means that some mechanism to decrease the oxide ion migration becomes evident at lower temperature such as a ordering or a clustering of defects, e.g. excess oxide ions.

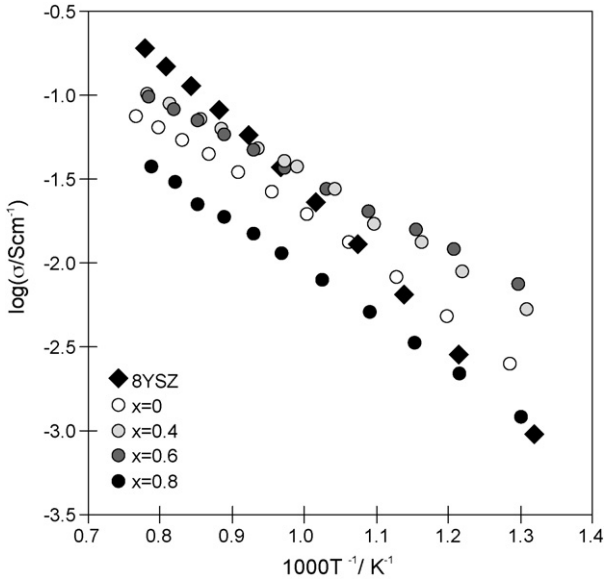

Fig. 5. The ionic conductivities of $La_{10-X}Ba_XSi_6O_{27}$ (X = 0, 0.4, 0.6, 0.8) and 8YSZ.

Fig. 6 shows the relation between the Ba contents and conductivity at 1000 °C. The conductivity increases with the Ba substitution, and $La_{10-X}Ba_XSi_6O_{27-X/2}$ sample with X = 0.6 shows the highest conductivity which is the same as 8YSZ at 750 °C and higher than 8YSZ below 700 °C because of the lower activation energy of the Ba substituted samples. As already described in the introduction, the conduction mechanism of this material is the interstitial diffusion of oxide ions. The substitution of Ba^{2+} at the La sites decreases the total oxide ions in a single cell, which leads to a decrease in the carrier density. The conductivity of the Ba substituted sample, however, shows a slight increase up to X = 0.6, which reveals that the carrier mobility is increased. As described in Structure analysis the lattice volume increases with the Ba substitution, which can explain the conductivity enhancement. Furthermore, a decrease in the occupation factor of the oxide ions of the SiO_4 tetrahedra may create the migration pathway to increase the conductivity perpendicular to the *c*-axis. The result of Table 1 showed that the oxide site

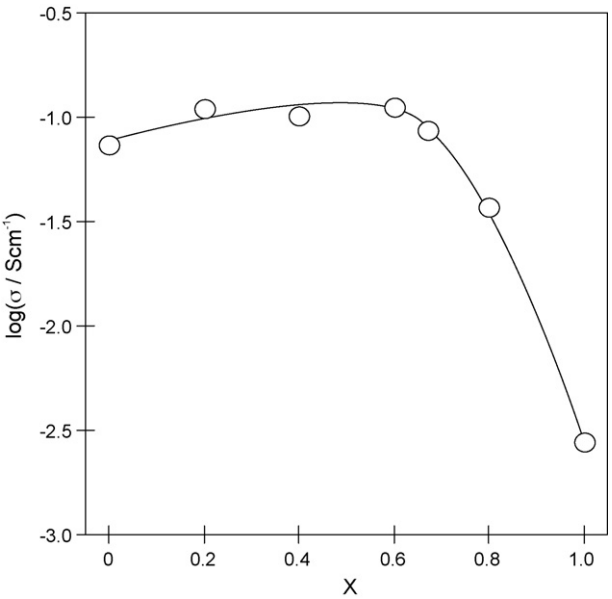

Fig. 6. The ionic conductivity of $La_{10-X}Ba_XSi_6O_{27}$ (X = 0–1.0) at 1000 °C.

Table 2
The activation energy of $La_{10-X}Ba_XSi_6O_{27-X/2}$ ($0 \le X \le 1.0$).

X	Inflection temperature (°C)	Activation energy (kJ mol^{-1})	
		High temperature	Low temperature
0	743	55.1	68.2
0.2	726	50.2	54.9
0.4	728	49.8	58.9
0.6		49.3	
0.8		63.4	
1.0		67.4	

occupation of the SiO_4 tetrahedra and the O4 sites were decreased by the Ba substitution. The opposite results are obtained at the isotropic temperature factor in Table 1. These results suggests that the spatial expanse of oxide ions are increased at the sites, and that the resulting increase of ionic conductivity happen at the *ab* plane and the *c*-axis.

With $X = 0.8$ and 1.0, the conductivity decreases and activation energy increases again. The result can be explained by a decrease in the total oxide ions, and excessive amounts of substituent leading to a decrease in the oxide ion conductivity by the formation of clusters of oxygen vacancies and substituent, which is already well known [30]. Furthermore, the result of structure analysis shows the change of the Ba substitution site. This result suggests that relation with decrease in the conductivity.

Table 2 shows the activation energy of $La_{10-X}Ba_XSi_6O_{27-X/2}$. The sample with $X = 0$ shows a higher activation energy than those with $X = 0.2$ to $X = 0.6$. The samples where X ranged from 0 to 0.4 exhibited an inflection in the activation energy. The samples with $X = 0.6$ to $X = 1.0$ did not show an inflection in the activation energy over the entire temperature range. The inflection temperatures of the samples decrease with an increase in X. Based on the discussion of the structural analysis, these activation energy results indicate that the Ba substitution in the La 4f site decreases the activation energy by forming a new pathway.

There was little difference, but both of the activation energy at high and low-temperature were decreased with an increase in X. These behaviors of the activation energy can be explained by the creation of the oxygen vacancies in the Ba substituted samples, and the same phenomenon has been already observed in the Ca substituted samples [24].

3.3. Fuel cell performance

Fig. 7 shows the fuel cell performances of the $La_{10}Si_6O_{27}$ and the $La_{9.4}Ba_{0.6}Si_6O_{26.7}$. The open circuit voltage (OCV) of 1.22–1.23 V are in good agreement with the theoretical value, which indicates that these samples are pure oxide-ion conductor. At a low current density, there was no activation overpotential in the *I–V* plots for the samples, which indicates that the oxide cathode and anode of these samples both acts as active electrodes [23].

The current density of $La_{10}Si_6O_{27}$ is 200 mA cm^{-2} which is almost double that of the Pt electrodes reported by Yoshioka and Tanase [16]. The maximum power density of $La_{10}Si_6O_{27}$ was 50 mW cm^{-2} which is 50% higher than the value using the Pt electrodes and measured at the same temperature [16]. $La_{9.4}Ba_{0.6}Si_6O_{26.7}$ exhibits higher current density of 230 mA cm^{-2} and a higher maximum power density of 65 mW cm^{-2}. The internal resistances of the SOFCs, which were calculated from the linear parts of the *I–V* curves, were 65 Ω cm for $La_{10}Si_6O_{27}$ and 51 Ω cm for $La_{9.4}Ba_{0.6}Si_6O_{26.7}$. Recent paper have reported 157 Ω cm for $La_{9.6}Si_{5.7}Mg_{0.3}O_{26.1}$ [17], and about 100 Ω cm for $La_{10}Si_6O_{27}$ [22]. A comparison of the internal resistance values of $La_{10}Si_6O_{27}$ indicated that there was high resistance area at the interface between an electrode and the electrolyte.

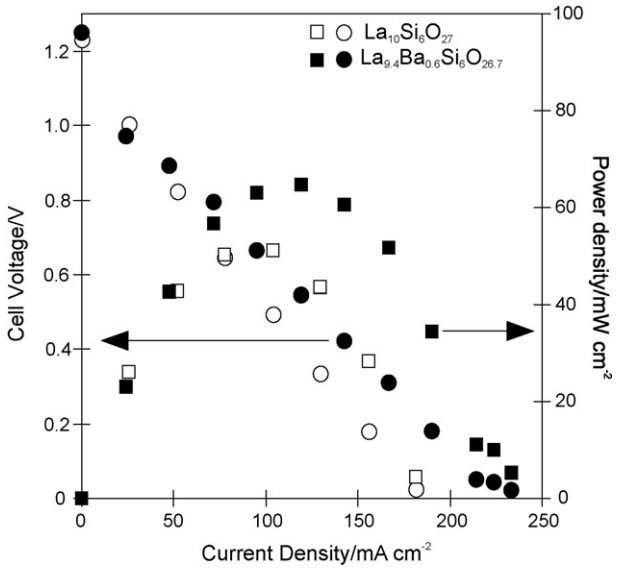

Fig. 7. The SOFC performances of $La_{10}Si_6O_{27}$ and $La_{9.4}Ba_{0.6}Si_6O_{26.7}$. The cathode and anode electrodes were $La_{0.9}Sr_{0.1}CoO_{3-\delta}$ and NiO-SDC, respectively.

Since we have not optimized the composition and calcination conditions of the electrodes, it is possible to obtain a higher power density in the future by optimizing them.

4. Conclusion

We investigated the relations between the Ba ion occupation sites and conductivity. A Rietveld analysis of the diffraction using synchrotron radiation showed that the Ba ion occupied the La 4f site in $La_{9.4}Ba_{0.6}Si_6O_{26.7}$. In addition, the presence of the Ba ion in the La 4f site caused oxygen defects in the SiO_4 tetrahedra, which produced an oxide ion path along the *a* and *b* axes in the crystal, thus enhancing the conductivity. On the other hand, in a composition where $X > 0.6$, there is a possibility for the Ba ions occupied the La 6h site and the La 4f site from the Rietveld analysis result of $X = 0.8$. Additionally, since the ionic radius of Ba is larger than that of La, it will give rise to an increase in the activation energy. The activation energies of the Ba substituted samples were lower than that of a blank sample, except when $X > 0.6$. This result may suggest the formation of a new carrier pathway by the Ba substitution in the samples. $La_{9.4}Ba_{0.6}Si_6O_{26.7}$ produced a maximum power density of 65 mW cm^{-2}. $La_{10}Si_6O_{27}$ produced a 50 mW cm^{-2} maximum power density. This result for $La_{10}Si_6O_{27}$ was 50% greater than that of a recent report, which was obtained using Pt electrodes. The internal resistances of the samples were lower than that of the Pt electrodes. This result indicates that a high resistance area may exist at the interface between an electrode and the electrolyte.

Acknowledgements

This work was partially supported by a Grant-in-Aid for Scientific Research on Priority Areas, "Panoscopic Formation Controls and Highly Functionalized Property Designs for Rare Earth Materials," from the Ministry of Education, Science, Sports and Culture, Japan. This work was also partially supported by a Grant-in-Aid for Young Scientists Start-up from the Ministry of Education, Science, Sports and Culture, Japan.

References

[1] J.W. Fergus, J. Power Sources 162 (2006) 30–40.
[2] S. Nakayama, T. Kageyama, H. Aono, Y. Sadaoka, J. Mater. Chem. 5 (1995) 1801–1805.
[3] S. Nakayama, H. Aono, Y. Sadaoka, Chem. Lett. 24 (6) (1995) 431–432.
[4] S. Nakayama, M. Sakamoto, J. Eur. Ceram. Soc. 18 (1998) 1413–1418.
[5] M. Higuchi, K. Kodaira, S. Nakayama, J. Cryst. Growth 207 (1999) 298–302.
[6] M. Higuchi, K. Kodaira, S. Nakayama, J. Cryst. Growth 216 (2000) 317–321.
[7] H. Arikawa, H. Nishiguchi, T. Ishihara, Y. Takita, Solid State Ionics 136–137 (2000) 31–37.
[8] H. Okudera, A. Yoshiasa, Y. Masubuchi, M. Higuchi, S. Kikkawa, J. Solid State Chem. 177 (2004) 4451–4458.
[9] V.V. Kharton, F.M.B. Marques, A. Atkinson, Solid State Ionics 174 (2004) 135–149.
[10] V.V. Kharton, A.L. Shaula, M.V. Patrakeev, J.C. Waerenborgh, F.M.B. Marques, J. Electrochem. Soc. 151 (2004) A1236–A1246.
[11] J.E.H. Sansom, J.R. Tolchard, P.R. Slater, M.S. Islam, Solid State Ionics 167 (2004) 17–22.
[12] A.A. Yaremchenko, A.L. Shaula, V.V. Kharton, J.C. Waerenborgh, D.P. Rojas, M.V. Patrakeev, F.M.B. Marques, Solid State Ionics 171 (2004) 51–59.
[13] A.L. Shaula, V.V. Kharton, F.M.B. Marques, J. Solid State Chem. 178 (2005) 2050–2061.
[14] H. Okudera, Y. Masubuchi, S. Kikkawa, A. Yoshiasa, Solid State Ionics 176 (2005) 1473–1478.
[15] J.E.H. Sansom, P.A. Sermon, P.R. Slater, Solid State Ionics 176 (2005) 1765–1768.
[16] H. Yoshioka, S. Tanase, Solid State Ionics 176 (2005) 2395–2398.
[17] H. Yoshioka, J. Alloys Compd. 408–412 (2006) 649–652.
[18] L. Leon-Reina, J.M. Porras-Vazquez, E.R. Losilla, M.A.G. Areanda, Solid State Ionics 177 (2006) 1307–1315.
[19] S. Lambert, A. Vincent, E. Bruneton, S. Beaudet-Savignat, F. Guillet, B. Minot, F. Bouree, J. Solid State Chem. 179 (2006) 2602–2608.
[20] A. Vincent, S.B. Savignat, F. Gervais, J. Eur. Ceram. Soc. 27 (2007) 1187–1192.
[21] L. Leon-Reina, J.M. Porras-Vazquez, E.R. Losilla, M.A.G. Aranda, J. Solid State Chem. 180 (2007) 1250–1258.
[22] T. Nakao, A. Mineshige, M. Kobune, T. Yazawa, H. Yoshioka, The Proceedings of 16th Solid State Ionics, Shanghai, 2007, p. 510.
[23] H. Yoshioka, Y. Nojiri, S. Tanase, Solid State Ionics 179 (2008) 2165–2169.
[24] P.J. Panteix, E. Béchade, I. Julien, P. Abélard, D. Bernache-Assollant, Mater. Res. Bull. 43 (2008) 1223–1231.
[25] A. Mineshige, T. Nakao, M. Kobune, T. Yazawa, H. Yoshioka, Solid State Ionics 179 (2008) 1009–1012.
[26] T. Nakao, A. Mineshige, M. Kobune, T. Yazawa, H. Yoshioka, Solid State Ionics 179 (2008) 1567–1569.
[27] R. Ali, M. Yashima, Y. Matsushita, H. Yoshioka, F. Izumi, J. Solid State Chem. 182 (2009) 2846–2851.
[28] G. Oehlschlegel, W. Ohnmacht, Glastech. Ber. 48 (11) (1975) 232–236.
[29] M.E. Huntelaar, E.H.P. Cordfunke, J. Nucl. Mater. 201 (1993) 250–253.
[30] I.R. Gibson, J.T.S. Irvine, J. Mater. Chem. 6 (1996) 895–898.
[31] F. Izumi, T. Ikeda, Mater. Sci. Forum 321–324 (2000) 198–203.